RSC Advances

PAPER

View Article Online
View Journal | View Issue

Cite this: *RSC Adv.*, 2021, **11**, 38632

Mesoporous silica shell-coated single gold nanorods as multifunctional orientation probes in dynamic biological environments†

Geun Wan Kim,[a] In-Seob Han*[b] and Ji Won Ha *[ac]

Received 1st September 2021
Accepted 19th November 2021

DOI: 10.1039/d1ra06572f

rsc.li/rsc-advances

Mesoporous silica shell-coated gold nanorods (AuNRs@mSiO$_2$) can be employed as promising multifunctional orientation probes in biological studies owing to their anisotropic optical properties, enhanced stability, excellent biocompatibility, *etc.* In this study, the optical properties of single AuNRs@mSiO$_2$ are characterized under dark-field and differential interference contrast (DIC) microscopy. Furthermore, we presented polarization-dependent, periodic DIC images and intensities of single AuNRs@mSiO$_2$ at their localized surface plasmon resonance wavelength and investigated their use as multifunctional orientation probes in dynamic biological environments. Moreover, the real-time rotational motions of the AuNRs@mSiO$_2$ on the HeLa cell membranes were tracked with millisecond temporal resolution. Overall, AuNRs@mSiO$_2$ demonstrated their capacity to act as multifunctional optical probes owing to the combined effect of the Au core, which can serve as an orientation probe and a local heat generator for phototherapy, and the mesoporous silica shell, which can be used as a reservoir of chemotherapeutics owing to its excellent loading capacity.

Introduction

Plasmonic gold nanorods (AuNRs) have numerous biomedical applications because of their unique shape-induced optical properties which can be attributed to the localized surface plasmon resonance (LSPR) effect, facile surface modification, *etc.*1–4 For example, AuNRs have been used in phototherapy[5–7] owing to their high efficiency in photothermal conversion and as local heat generators in chemotherapy treatments to activate and enhance photothermally induced drug release.[8,9]

Despite their merits for biomedical applications, the presence of highly toxic cetyltrimethylammonium bromide (CTAB) bilayers used in the seed-mediated growth strategy limits the direct use of AuNRs.[10] Thus, the surface functionalization of AuNRs is mandatory to improve their biocompatibility. Recently, mesoporous silica shell-coated AuNRs (AuNRs@mSiO$_2$, core@shell) have exhibited excellent biocompatibility.[11] Furthermore, they can be used for synergistic phototherapy and chemotherapy combination using the mesoporous silica pores as reservoirs for chemotherapeutics owing to their high loading capacity, while the AuNRs serve as a local heat generator to induce phototherapy and trigger drug release.[11–16]

AuNRs have also been effectively used as orientation probes with a few polarization-based optical techniques, including dark-field (DF) polarization microscopy,[17] photothermal heterodyne imaging (PHI),[18] differential interference contrast (DIC) polarization anisotropy,[1,19] and total internal reflection (TIR) scattering microscopy.[20–22] Therefore, AuNRs@mSiO$_2$ can be used as multifunctional optical probes in biological studies. For example, the AuNR core can serve as an orientation probe and a heat generator in phototherapy, whereas the mesoporous silica shell can be used as a chemotherapeutics reservoir.[11,13,15] However, our understanding of their use as multifunctional orientation probes is still limited in dynamic biological environments.

The scattering-based methods, such as DF microscopy, are challenging for identifying AuNRs from cellular components and other debris that scatter light. In this regard, interference-based DIC microscopy is more suitable for investigating rotational motions of AuNRs in biological environments.

In the present study, we aim to investigate the optical properties of single AuNRs@mSiO$_2$ in DF and DIC microscopy. The effect of light polarization on the DIC image patterns and intensities of single AuNRs@mSiO$_2$ at their LSPR wavelengths is observed, and their potential use for the development of multifunctional orientation probes in dynamic biological environments is examined under a DIC microscope.

[a]*Department of Chemistry, University of Ulsan, 93 Daehak-ro, Nam-gu, Ulsan, 44610, Republic of Korea. E-mail: jwha77@ulsan.ac.kr; Fax: +82 52 712 8002; +82 52 259 1694; Tel: +82 52 712 8012; +82 52 259 2352*

[b]*School of Biological Sciences, University of Ulsan, 93 Daehak-ro, Nam-gu, Ulsan, 44610, Republic of Korea. E-mail: hanis@ulsan.ac.kr*

[c]*Energy Harvest-Storage Research Center (EHSRC), University of Ulsan, 93 Daehak-ro, Nam-gu, Ulsan, 44610, Republic of Korea*

† Electronic supplementary information (ESI) available. See DOI: 10.1039/d1ra06572f

Experimental section

Materials and chemicals

AuNRs@mSiO$_2$ were purchased from Nanopartz (Loveland, CO, USA). The cervical carcinoma cell line, HeLa-WT, was obtained from the Korean Cell Line Bank (Seoul, South Korea). Fetal bovine serum (FBS) was purchased from Sigma-Aldrich (St. Louis, MO, USA). Deionized water (18.2 MΩ cm) was prepared using a Sartorius Arium®Pro Ultrapure water system.

Sample preparation and characterization

The AuNRs@mSiO$_2$ solution was diluted with 18.2 MΩ pure water to the proper concentration and then sonicated for 15 min at room temperature. The samples were prepared by spin-casting the solution on the precleaned glass slide and covered with a 22 mm × 22 mm No 1.5 coverslip. The concentration of AuNRs@mSiO$_2$ on the glass surface was controlled to be ∼1 μm^{-2} to facilitate single-particle characterization and to minimize interparticle LSPR coupling. Structural characterization was performed using a transmission electron microscope (TEM; H-8100, HITACHI, JAPAN) and a scanning electron microscope (SEM; JSM-6500, JEOL, JAPAN).

Cell culture

The HeLa cells were placed in a cell culture flask and grown in a cell culture medium supplemented with 10% FBS in a cell culture incubator (37 °C, 5% CO_2) for 24 h. For sub-culturing, 200 μL of the cell suspension was transferred to a 22 × 22 mm^2 No 1.5 poly-L-lysine-coated coverslip (Corning, NY) and stored in a Petri dish, which was then incubated for 1 h to allow the cells to attach to the coverslip. The coverslip was covered with 1.5 mL of the cell culture medium containing 10% FBS supplement, and the Petri dish was placed in the incubator for 24 h.

DF microscopy and spectroscopy

DF microscopy was performed under a Nikon inverted microscope (ECLIPSE Ti-U). In DF mode, the microscope utilized a Nikon Plan Fluor 100 × 0.5–1.3 oil iris objective and a Nikon DF condenser. An Andor iXon^{EM} + CCD camera (iXon Ultra 897) was employed to record DF images of AuNRs@mSiO$_2$, which were analyzed using Image J. DF scattering spectra were measured and captured using an Andor spectrometer (SHAMROCK 303i, SR-303I-A) and an Andor CCD camera (Newton DU920P-OE). The scanning stage moved the sample to the desired location so that only the scattered light from the selected location was collected by the objective for spectral measurement. The scattered light was directed to the entrance of the spectrometer, dispersed by a grating (300 l mm^{-1}), and detected by the Newton CCD camera. The background was measured at a region without any particles. Data analysis was performed with specially designed MATLAB programs.

Differential interference contrast microscopy

DIC microscopy was performed using a Nikon inverted microscope (ECLIPSE Ti-U) comprising two Normarski prisms, two polarizers, and a quarter waveplate. The samples were illuminated through an oil immersion condenser (numerical aperture (NA) = 1.4). The signals that passed through the sample were collected using a Plan Apo oil-immersion objective (100×, NA = 1.4). A bandpass filter with a 720 nm central range (full width at half maximum, ±5 nm) was obtained from Thorlabs (Newton, NJ, USA) and inserted into the beam path of the microscope to illuminate the samples. A rotational study was conducted at 720 nm excitation by rotating the stage 10° per step for single AuNRs@mSiO$_2$. The fixed AuNRs@mSiO$_2$ were positioned in different orientations as the stage was rotated. The Andor iXon^{EM} + CCD camera was used to record highly detailed DIC images of the AuNRs@mSiO$_2$, which were analyzed using Image J.

Results and discussion

TEM and SEM images of single AuNRs@mSiO$_2$ are shown in Fig. 1A and S1 (of the ESI†), respectively. The average width and length of AuNRs@mSiO$_2$ were 40 nm and 120 nm, respectively. In the ultraviolet–visible light extinction spectrum of AuNRs@mSiO$_2$ dispersed in water, shown in Fig. 1B, the transverse and longitudinal LSPR peaks were observed at 526 and 723 nm, respectively. The thickness of silica shell was approximately 18 nm.

We performed single-particle measurements using the experimental setup shown in Fig. S2† to understand the scattering properties of AuNRs@mSiO$_2$ and eliminated the effect of averaging under DF scattering microscopy and spectroscopy. The AuNRs@mSiO$_2$ were illuminated with a randomly polarized white light tightly focused using a high NA oil condenser under DF microscopy. A DF scattering image of two AuNRs@mSiO$_2$ (labeled as AuNR1@mSiO$_2$ and AuNR2@mSiO$_2$ and marked with yellow squares) deposited on a glass slide are shown in Fig. 2A; single-particle scattering spectra of the two highlighted nanorods are shown in Fig. 2B. The LSPR wavelength of the single AuNRs@mSiO$_2$ in the single-particle spectra appeared at 690–760 nm, which can be ascribed to heterogeneity in particle

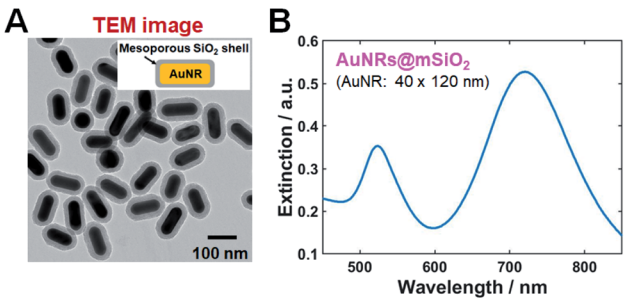

Fig. 1 (A) TEM image of AuNRs@mSiO$_2$. The average length and width are 120 and 40 nm, respectively. The inset illustrates the AuNRs@mSiO$_2$. (B) Normalized ultraviolet–visible (UV-Vis) extinction spectrum of AuNRs@mSiO$_2$ dispersed in water.

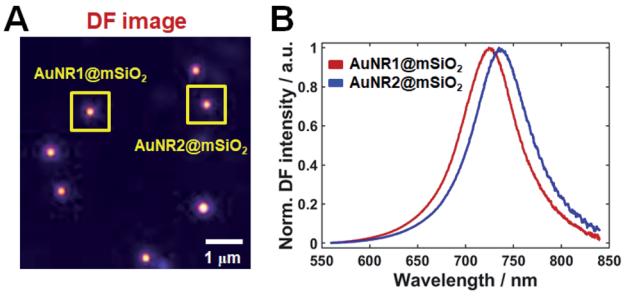

Fig. 2 (A) DF image of single AuNRs@mSiO$_2$ on a glass slide. (B) Single-particle scattering spectra of the two AuNRs@mSiO$_2$ (AuNR1@mSiO$_2$, AuNR2@mSiO$_2$) marked with a yellow square in (A).

size (see also Fig. S3†). This result from the single-particle measurements is consistent with the result from the ensemble experiments shown in Fig. 1B.

DIC microscopy is better suited to probe orientation and rotational motion of nanoprobes in live cells.[3,23–25] DIC microscopy resolves the optical path difference between two mutually orthogonally polarized beams separated by a shear distance along the optical axis of a Nomarski prism (see Fig. S4†), making it insensitive to scattered light from surrounding cellular components while maintaining its high-throughput capability. Therefore, the DIC microscopy-based single-particle rotational tracking technique is effectively used in studies of the rotational dynamics in live cells.

The optical properties of single AuNRs@mSiO$_2$ fixed on a glass slide were then examined under DIC microscopy at 720 nm excitation close to their longitudinal LSPR wavelength; a DIC image of single AuNRs@mSiO$_2$ on a glass slide at 720 nm is shown in Fig. 3A. The orientation of the AuNR core inside the silica shell was defined as the orientation angle φ between the longitudinal axis of AuNR and dark axis, as shown in the inset of Fig. 3A. The orientation angle increased in the counterclockwise direction toward the bright axis. Different DIC image patterns of single AuNRs@mSiO$_2$ were observed owing to their spatial orientation on the glass slide; *i.e.*, a bright image pattern was observed for AuNR3@mSiO$_2$ since it was aligned parallel to the bright polarization axis ($\varphi = 90°$, blue arrow), whereas a dark image pattern was observed for AuNR4@mSiO$_2$. Therefore, DIC microscopy facilitated orientation-dependent DIC image patterns of single AuNRs@mSiO$_2$ to be observed with high contrast and sensitivity. The scattering spectrum of the AuNR3@mSiO$_2$ highlighted by a yellow square in Fig. 3A was obtained to confirm that it was a single nanoparticle rather than an aggregate and is shown in Fig. 3B. The measured longitudinal LSPR peak of AuNR3@mSiO$_2$ appeared at 720 nm, which is consistent with the single-particle spectra in Fig. 2B and S3.† Next, polarization-dependent DIC imaging was performed for the fixed AuNR3@mSiO$_2$ at an excitation of 720 nm by rotating the stage 10° per step to position AuNR3@mSiO$_2$ in different orientations. The complete set of obtained DIC images of AuNR3@mSiO$_2$ from 0° to 180° at intervals of 10° is shown in Fig. 3C, where the image patterns periodically changed as a function of the rotation angle. Polarization-dependent DIC images of AuNR4@mSiO$_2$ marked in Fig. 3A are also provided in Fig. S5.†

The normalized DIC intensities of AuNR3@mSiO$_2$ for two bright (blue) and dark (red) polarization directions were then plotted as a function of rotation angle in Fig. 4A to gain a deeper insight into the polarization dependence. As the stage was rotated, the DIC bright (red) and dark (blue) intensity curves

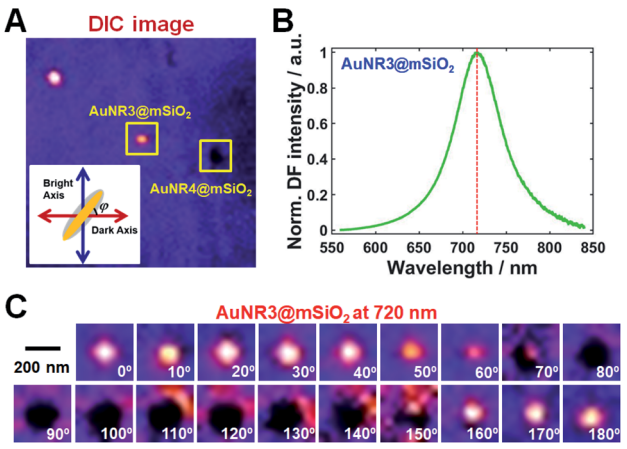

Fig. 3 (A) DIC image of single AuNRs@mSiO$_2$ with different orientations on a glass slide. The AuNRs@mSiO$_2$ were illuminated at their longitudinal SPR wavelength of 720 nm. The inset represents the definition of the orientation angle φ of a AuNR@mSiO$_2$ with respect to the dark polarization axis. (B) Single-particle scattering spectrum of AuNR3@mSiO$_2$, highlighted by the yellow square in (A). The longitudinal SPR peak was observed at approximately 720 nm. (C) Polarization-dependent DIC images of single AuNR3@mSiO$_2$ obtained by rotating the stage in increments of 10° at 720 nm excitation.

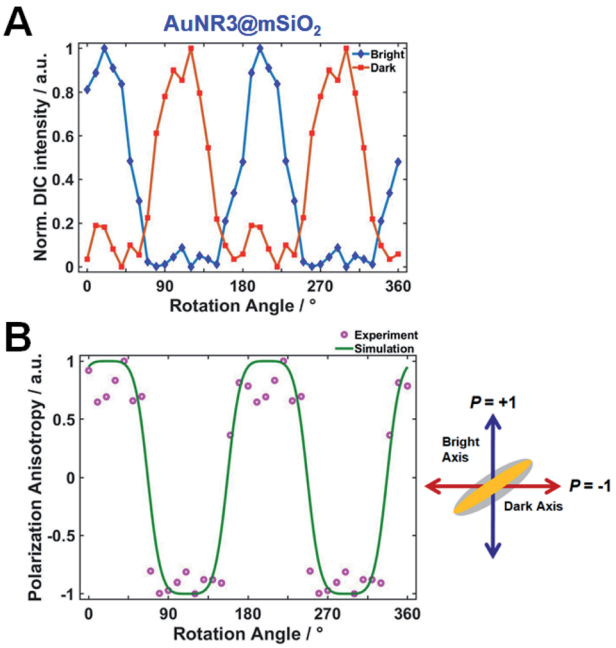

Fig. 4 (A) DIC intensity profiles and (B) polarization anisotropy P of AuNR3@mSiO$_2$ as a function of rotation angle. In (B), the experimental values of P (pink dots) fit the calculated P values well (green curve).

were anticorrelated, *i.e.*, an increase in the bright intensity was accompanied by a decrease in the dark intensity, and *vice versa*. These observed polarization-sensitive, periodic DIC images and intensities of single AuNRs@mSiO$_2$ indicate that the spatial orientation of single AuNRs@mSiO$_2$ can be determined *via* DIC microscopy and polarization anisotropy (also see Fig. S5†).

DIC polarization anisotropy using an intensity ratio instead of absolute intensities is less affected by intensity instabilities and can thus provide more accurate, reproducible, and reliable angle measurements.[1,3,19] The DIC polarization anisotropy P can be obtained from the bright and dark intensities of a single DIC image of the AuNR@mSiO$_2$, as[19]

$$P = \frac{I_{B,N} - I_{D,N}}{I_{B,N} + I_{D,N}} \quad (1)$$

where $I_{B,N}$ and $I_{D,N}$ are the normalized bright and dark intensities, respectively. The calculated DIC polarization anisotropy P of AuNR3@mSiO$_2$ as a function of orientation angle φ is shown in Fig. 4B, where the DIC polarization anisotropy P oscillated between minimum and maximum values of -1 and $+1$ depending on the orientation. P reached the maximum value of $+1$ when AuNR3@mSiO$_2$ was aligned parallel to the bright axis. As shown in Fig. 4B and S5C,† the experimental P values obtained from eqn (1) agreed well with the calculated P values, thereby validating that DIC polarization anisotropy allows for accurate measurements of the orientation angles of single AuNRs@mSiO$_2$. The DIC polarization anisotropy P can be related to the orientation angle φ, as

$$\varphi = \operatorname{acos}\left(\sqrt{\frac{A - \sqrt{A^2 - 2A}}{2}}\right), \quad P < 0$$
$$\varphi = \operatorname{acos}\left(\sqrt{\frac{A + \sqrt{A^2 - 2A}}{2}}\right), \quad P > 0 \quad (2)$$

where A is defined as $(P-1)/P$. Thus, the orientation angle φ can be obtained from a measured DIC polarization anisotropy P.

To compare with single AuNRs@mSiO$_2$, we further obtained DIC images of an aggregate by rotating the stage with increments of 10° (Fig. S6†). Unlike single AuNRs@mSiO$_2$, the DIC image patterns and intensities of the aggregate were not periodically changed as a function of rotational angle. Thus, we were not able to observe polarization-dependent DIC images and intensities in case of the aggregate.

Next, we tested if the DIC polarization anisotropy can be used to track fast rotational dynamics of single AuNRs@mSiO$_2$ in real-time. Thus, we chose single AuNRs@mSiO$_2$ rotating on a glass slide as a model system to verify. We observed that some AuNRs@mSiO$_2$ were attached on a glass slide through non-specific binding (Fig. 5, Movies S1 and S2†) and showed fast rotational motions. As shown in Fig. 5C, the experimental P values were randomly changed over time in between -1 and $+1$ depending on the orientation of AuNR5@mSiO$_2$. Therefore, we demonstrated that the DIC polarization anisotropy can be used to determine the orientation angles of single AuNRs@mSiO$_2$ in fast rotational motions.

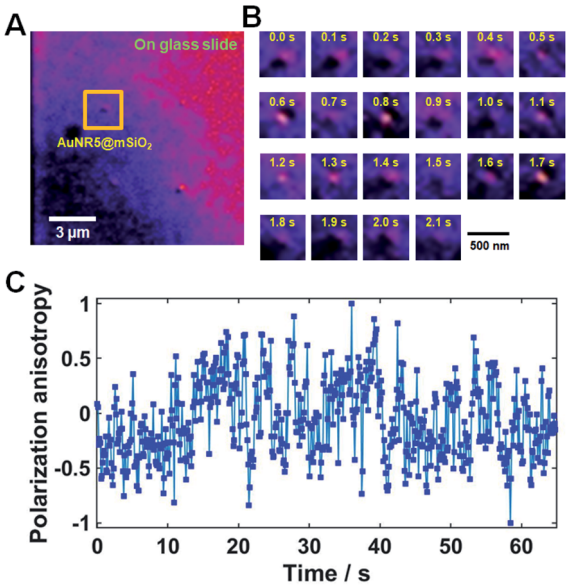

Fig. 5 (A) DIC image of AuNR5@mSiO$_2$ bound onto a glass slide. (B) 22 successive DIC images of AuNR5@mSiO$_2$ chosen from Movie S2.† The temporal resolution was 100 ms. (C) DIC polarization anisotropy P for AuNR5@mSiO$_2$ as a function of time for all consecutive frames in Movie S2.†

The next crucial step was to verify that single AuNRs@mSiO$_2$ could be used as high-contrast multifunctional orientation probes in dynamic biological environments under DIC microscopy. In recent studies, single AuNRs@mSiO$_2$ have been employed as efficient drug delivery cargoes in biological applications.[11,13–15,26] Tracking rotational and translational dynamics of individual AuNRs@mSiO$_2$ on live cell membranes will provide a better understanding of drug delivery mechanisms and other cellular processes, such as endocytosis. AuNRs@mSiO$_2$ rotating on live cell membranes were thus used as a model system to verify their use as multifunctional orientation probes in dynamic biological systems.

The rotational motions of surface-bound AuNRs@mSiO$_2$ were recorded at a temporal resolution of 100 ms under DIC microscopy, as shown in Movie S3.† The AuNR6@mSiO$_2$ rotated quickly when it first fell on the HeLa cell membrane, as revealed by an image flicker. A captured DIC image of AuNR6@mSiO$_2$ bound to a live cell membrane is shown in Fig. 6A. The DIC image patterns changed dynamically as a function of time, as demonstrated by the 20 consecutive frames from Movie S3† shown in Fig. 6B. The DIC polarization anisotropy P values for these 20 images were randomly distributed between -1 and $+1$, as demonstrated in Fig. 6C. More experimental data for AuNR7@mSiO$_2$ and AuNR8@mSiO$_2$ rotating on the live cell membrane are provided in Fig. S7 and S8.† The results support the utility of single AuNRs@mSiO$_2$ as orientation probes under DIC microscopy and demonstrate that DIC polarization anisotropy allows precise determination of their real-time orientation during dynamic biological processes.

Further, AuNRs@mSiO$_2$ present two main advantages over bare AuNRs (no silica shell) that have been conventionally used

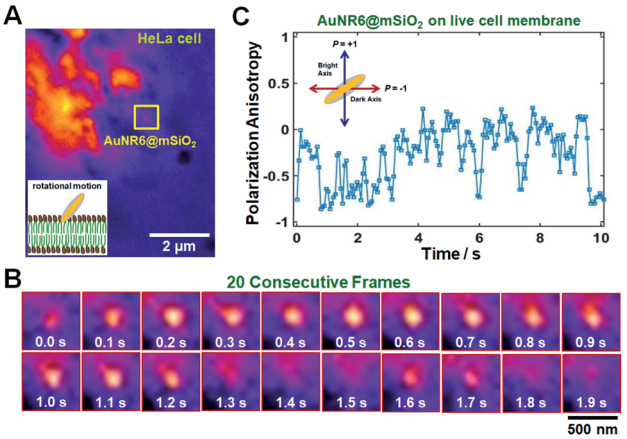

Fig. 6 (A) DIC image of AuNR6@mSiO$_2$ bound onto a live cell membrane. (B) 20 successive DIC images of AuNR6@mSiO$_2$ chosen from Movie S3.† The temporal resolution was 100 ms. (C) DIC polarization anisotropy P for AuNR6@mSiO$_2$ as a function of time for all consecutive frames in Movie S3.† The inset shows a schematic of P values for two special cases ($\varphi = 0°$ and $\varphi = 90°$).

as orientation probes in biological studies, whose orientation angles can both be obtained with high sensitivity under DIC microscopy. First, AuNRs@mSiO$_2$ can be used as multifunctional orientation probes because of the added functions compared with the bare AuNR probe.[27,28] For example, the mesoporous silica shell in a drug delivery system can provide excellent loading capacity, reduced toxicity, and enhanced stability. Second, as demonstrated in Fig. 5, the Au core inside the silica shell can be used as an orientation probe and a local heat generator to induce phototherapy in biological systems. Therefore, AuNRs@mSiO$_2$ can be used as multifunctional orientation probes in various biomedical studies.

Conclusions

In summary, the optical properties of single AuNRs@mSiO$_2$ at their LSPR wavelengths under DF and DIC microscopy and their use as orientation probes in dynamic biological systems were examined. Single AuNRs@mSiO$_2$ showed polarization-sensitive, periodic DIC images and intensities at their LSPR wavelengths with high contrast and sensitivity. We for the first time described a real-time tracking of the rotational motions of AuNRs@mSiO$_2$ on live cell membranes under DIC microscopy to verify the capability of single AuNRs@mSiO$_2$ as multifunctional orientation probes. The results presented here support the potential use of single AuNRs@mSiO$_2$ for the development of multifunctional orientation probes owing to the combined effect of the Au core, which can serve as an orientation probe and a local heat generator for phototherapy, and mesoporous silica shell, which can be used as efficient drug carriers due to its excellent loading capacity in many biological applications.

Conflicts of interest

There are no conflicts to declare.

Acknowledgements

This work was supported by two National Research Foundation of Korea (NRF) grants funded by the Korean government (MSIP) (No 2018R1C1B3001154 and No 2019R1A6A1A11053838).

Notes and references

1 J. W. Ha, W. Sun, A. S. Stender and N. Fang, *J. Phys. Chem. C*, 2012, **116**, 2766–2771.
2 Z. Ma, H. Xia, Y. Liu, B. Liu, W. Chen and Y. Zhao, *Chin. Sci. Bull.*, 2013, **58**, 2530–2536.
3 L. Xiao, J. W. Ha, L. Wei, G. Wang and N. Fang, *Angew. Chem., Int. Ed.*, 2012, **51**, 7734–7738.
4 R. A. Sperling, P. R. Gil, F. Zhang, M. Zanella and W. J. Parak, *Chem. Soc. Rev.*, 2008, **37**, 1896–1908.
5 M. R. K. Ali, Y. Wu and M. A. El-Sayed, *J. Phys. Chem. C*, 2019, **123**, 15375–15393.
6 K. Turcheniuk, T. Dumych, R. Bilyy, V. Turcheniuk, J. Bouckaert, V. Vovk, V. Chopyak, V. Zaitsev, P. Mariot, N. Prevarskaya, R. Boukherroub and S. Szunerits, *RSC Adv.*, 2016, **6**, 1600–1610.
7 X. Kang, X. Guo, X. Niu, W. An, S. Li, Z. Liu, Y. Yang, N. Wang, Q. Jiang, C. Yan, H. Wang and Q. Zhang, *Sci. Rep.*, 2017, **7**, 42069.
8 M. Zan, J. Li, M. Huang, S. Lin, D. Luo, S. Luo and Z. Ge, *Biomater. Sci.*, 2015, **3**, 1147–1156.
9 X. Wu, J. Liu, L. Yang and F. Wang, *Colloids Surf., B*, 2019, **175**, 239–247.
10 J. Wan, J.-H. Wang, T. Liu, Z. Xie, X.-F. Yu and W. Li, *Sci. Rep.*, 2015, **5**, 11398.
11 C. Li, K. Feng, N. Xie, W. Zhao, L. Ye, B. Chen, C.-H. Tung and L.-Z. Wu, *ACS Appl. Nano Mater.*, 2020, **3**, 5070–5078.
12 N. T. Ha Lien, A. D. Phan, B. T. Van Khanh, N. T. Thuy, N. Trong Nghia, H. T. My Nhung, T. Hong Nhung, D. Quang Hoa, V. Duong and N. Minh Hue, *ACS Omega*, 2020, **5**, 20231–20237.
13 G. Liu, H. Liang, Y. He, L. Lu, L. Wang, P. Liu and K. Cai, *J. Mater. Chem. B*, 2020, **8**, 9686–9696.
14 J. Liu, C. Detrembleur, M.-C. De Pauw-Gillet, S. Mornet, C. Jérôme and E. Duguet, *Small*, 2015, **11**, 2323–2332.
15 A. S. Monem, N. Elbialy and N. Mohamed, *Int. J. Pharm.*, 2014, **470**, 1–7.
16 X. Cui, W. Cheng and X. Han, *J. Mater. Chem. B*, 2018, **6**, 8078–8084.
17 C. Sönnichsen and A. P. Alivisatos, *Nano Lett.*, 2004, **5**, 301–304.
18 W.-S. Chang, J. W. Ha, L. S. Slaughter and S. Link, *Proc. Natl. Acad. Sci. U. S. A.*, 2010, **107**, 2781–2786.
19 J. W. Ha, W. Sun, G. Wang and N. Fang, *Chem. Commun.*, 2011, **47**, 7743–7745.
20 J. W. Ha, K. Marchuk and N. Fang, *Nano Lett.*, 2012, **12**, 4282–4288.
21 K. Marchuk and N. Fang, *Nano Lett.*, 2013, **13**, 5414–5419.
22 K. Marchuk, J. W. Ha and N. Fang, *Nano Lett.*, 2013, **13**, 1245–1250.

23 Y. Gu, J. W. Ha, A. E. Augspurger, K. Chen, S. Zhu and N. Fang, *Nanoscale*, 2013, **5**, 10753–10764.
24 Y. Gu, W. Sun, G. Wang and N. Fang, *J. Am. Chem. Soc.*, 2011, **133**, 5720–5723.
25 G. Wang, W. Sun, Y. Luo and N. Fang, *J. Am. Chem. Soc.*, 2010, **132**, 16417–16422.
26 Z. Song, Y. Liu, J. Shi, T. Ma, Z. Zhang, H. Ma and S. Cao, *Mater. Sci. Eng. C*, 2018, **83**, 90–98.
27 G. W. Kim, S. Y. Lee and J. W. Ha, *Analyst*, 2017, **142**, 899–903.
28 S. Y. Lee and J. W. Ha, *Phys. Chem. Chem. Phys.*, 2016, **18**, 32682–32685.